Combined SMAP/SMOS Thin Sea Ice Thickness Retrieval

Cătălin Paţilea[1], Georg Heygster[1], Marcus Huntemann[2,1], and Gunnar Spreen[1]

[1]Institute of Environmental Physics, University of Bremen, Bremen, Germany
[2]Alfred Wegener Institute, Bremerhaven, Germany

Correspondence to: Cătălin Paţilea (cpatilea@iup.physik.uni-bremen.de)

Abstract. The spaceborne passive microwave sensors Soil Moisture Ocean Salinity (SMOS) and Soil Moisture Active Passive (SMAP) provide brightness temperature data at L-band (1.4 GHz). At this low frequency the atmosphere is close to transparent and in polar regions the thickness of thin sea ice can be derived. SMOS data covers a large incidence angle range whereas SMAP observes at a fixed 40° incidence angle which makes thin sea ice thickness retrieval more consistent as incidence angle effects do not have to be taken into account. Here we transfer a retrieval algorithm for thickness of thin sea ice (up to 50 cm) from SMOS data at 40° to 50° incidence angle to the fixed incidence angle of SMAP. Now the SMOS brightness temperatures (TBs) at a given incidence angle are estimated using empirical fit functions. SMAP TBs are calibrated to SMOS for providing a merged SMOS/SMAP Sea Ice Thickness product.

1 Introduction

Sea ice is an important climate parameter (Moritz et al., 2002; Stroeve et al., 2007; Holland et al., 2010) and accurate knowledge of sea ice properties is needed for weather and climate modeling and prediction and for ship routing. The thickness of the ice is one of the parameters that determines resistance against the deforming forces of wind and ocean currents (Häkkinen, 1987; Yu et al., 2001). Even a thin layer of sea ice inhibits evaporation, reduces heat and gas exchange between ocean and atmosphere and increases the albedo (Maykut, 1978; Perovich et al., 2012). It provides a solid surface for snow to deposit, which further reduces heat exchange and increases albedo.

The Soil Moisture Ocean Salinity (SMOS) satellite was launched by ESA in November 2009. It is a synthetic aperture passive microwave radiometer working at L-band (1.4 GHz). The aperture synthesis requires an array of small antennas reducing the total weight and size of the satellite. The instrument works in a full polarimetric mode, recording all four Stokes parameters. Its large field of view allows for multi angular observations organized in an approximately 1200 km × 1200 km snapshots.

SMOS has been developed for retrieving soil moisture (Kerr et al., 2012), by inferring the surface emissivity which is correlated with the moisture content, and sea surface salinity (Zine et al., 2008; Font et al., 2010) where the measured brightness temperatures (TB) are linked with the sea salinity through the dielectric constant of the water in the first few centimeters. Modeling and observations showed that at this frequency the radiation is sensitive to ice thickness up to 0.5 meters (Kaleschke et al., 2010, 2012). The atmosphere has little influence on the radiation at L-band as both absorption and scattering are small (Skou and Hoffman-Bang, 2005). The correlation of ice thickness with emitted radiation together with a small atmospheric contribution make SMOS a candidate for thickness retrieval of thin sea ice. To date, two retrieval algorithms have been devel-

oped for SMOS, one using the intensity averaged over incidence angles between 0° and 40° (Tian-Kunze et al., 2014) and one using intensity and polarization difference averaged over incidence angles between 40° and 50° (Huntemann et al., 2014).

In 2015 the Soil Moisture Active Passive (SMAP) satellite was launched by NASA (Entekhabi et al., 2010, 2014). It carries two sensors onboard, a L-band radiometer, and a radar which share a rotating 6 m real aperture antenna reflector. The radar was recording high resolution (1 to 3 km) data used for soil moisture sensing, until it failed after three months. In contrast to the synthetic aperture observations of SMOS, the real aperture antenna observations of SMAP cover an area of 36 km × 47 km at a fixed incidence angle of 40° and results in a swath with an approximate width of 1000 km. SMAP also includes on board detection and filtering of Radio Frequency Interference (RFI) while SMOS does not.

After the launch of SMAP, different approaches were taken to convert data products between the two sensors. A previous approach to convert SMOS to SMAP TBs for usage in soil moisture retrieval and assimilation systems is presented in Lannoy et al. (2015) and involves a quadratic fitting of the SMOS TBs at the SMAP incidence angle and employing auxiliary data and an empirical atmospheric model to correct for the atmospheric and extraterrestrial contributions, respectively. In contrast, Huntemann et al. (2016) convert SMAP 40° surface TBs to SMOS top of the atmosphere equivalent 40 to 50° averaged TBs through two linear regressions.

In this article, we present a Sea Ice Thickness (SIT) dataset combining data of the two sensors by calibrating the SMAP brightness temperatures to those of SMOS (Sect. 4). As a first step, an inter-calibration of the brightness temperatures of the two sensors is required due to a possible warm bias in SMOS data (Sect. 2) and due to corrections for galactic noise and sun specular reflection contained in the SMAP but not in the SMOS data. In addition, the SIT retrieval from Huntemann et al. (2014) is adapted to the new version 6.20 of the SMOS Level 1C data and it will be used as a reference for all other comparisons (Sect. 3.1). This new retrieval is combined with a fit function for the dependence of horizontal and vertical brightness temperatures (from now on referred as TB_h and TB_v, respectively) on the incidence angle (Sect. 3.2). The fit function is used for RFI filtering and for SIT retrieval at a fixed incidence angle. The fit is also a step required for the SMOS and SMAP merged product to combine the observations of the two sensors at a common incidence angle.

2 SMOS and SMAP data sources

The MIRAS radiometer onboard the SMOS satellite has 69 receivers on three arms measuring radiances at 1.4 GHz (Kerr et al., 2001). One complete set of data from the aperture synthesis process done each 1.2 seconds is called a snapshot. For this investigation the SMOS Level 1C sea data gridded on the icosahedron Snyder equal area (ISEA) 4H9 grid (Sahr et al., 2003) is used. Its resolution is 15 km while the SMOS footprint size varies with incidence angle from approximately 30 km×30 km at nadir to 90 km×30 km at 65° (Castro, 2008). Over the whole field of view the average resolution is approximately 43 km. The Level 1C data is provided within 24 h of acquisition.

In full polarization mode, all four Stokes parameters are measured. Data is recorded in the reference plane of the antenna as T_X, T_Y, T_3 and T_4, and is converted to TB_h, TB_v, TB_3 and TB_4 in the Earth surface plane (Zine et al., 2008) using

$$\begin{bmatrix} T_X \\ T_Y \\ T_3 \\ T_4 \end{bmatrix} = \begin{bmatrix} \cos^2(\alpha) & \sin^2(\alpha) & -\cos(\alpha)\sin(\alpha) & 0 \\ \sin^2(\alpha) & \cos^2(\alpha) & \cos(\alpha)\sin(\alpha) & 0 \\ \sin(2\alpha) & -\sin(2\alpha) & \cos(2\alpha) & 0 \\ 0 & 0 & 0 & 1 \end{bmatrix} \begin{bmatrix} TB_h \\ TB_v \\ TB_3 \\ TB_4 \end{bmatrix}, \quad (1)$$

where $\alpha = \alpha_{gr} + \omega_{F_r}$, α_{gr} is the georotation angle and ω_{F_r} is the Faraday rotation angle. Within a snapshot just one or two of the Stokes parameters are measured at the same time. When only one of the Stokes parameters is measured, all three arms of the sensor record the same polarization. In the case of recording a cross-polarized snapshot, one arm of the sensor records one polarization while the other two record the other polarization. Measurements of single (XX or YY) and cross-polarization ((XX,XY) or (YY,XY)) are done alternatively. In order to obtain the values for TB_h and TB_v from the matrix, depending if the current measurement is single or cross-polarization, we will have to use one or two adjacent snapshots. The missing values required for the conversion are interpolated from neighboring snapshots within a 2.5 s range and with a maximum incidence angle difference between the measurements of 0.5°.

The SMOS L1C data version 6.20 has been operationally available since 5 May 2015 and also older acquisitions were reprocessed. This version adds better RFI flagging and it improves the long-term and seasonal stability of the measurements. At the same time it introduces a warm bias in the brightness temperatures of approximately 1.4 K relative to the previous version 5.05 over ocean. The bias over the ocean can be 1 K too warm with respect to the true values (SMOS Calibration team and Expert Support Laboratory Level 1, 2015). Over Antarctica and land, the bias is above 2 K, which is closer to modeled and ground based measurements. The new data version also reduces the difference in brightness temperature between ascending and descending overflights over ocean at low latitudes. At high latitudes such changes were not documented. Before, the difference varied considerably with time and latitude due to thermal variations in the instrument.

The SMAP satellite is positioned on a quasi-polar sun-synchronous orbit with ascending equator crossing time 6 pm, while SMOS has an equator crossing time at 6 am. SMAP carries a conically scanning radiometer with a fixed incidence angle of 40° which leads to a narrower swath and decreases the area covered at the pole compared to SMOS. The footprint of a SMAP observatoin is approximately 36 km × 47 km, resulting in an approximate resolution of 40 km.In this study, the SMAP Level 1B data is used which contains time ordered ungridded Top Of the Atmosphere (TOA) brightness temperatures. The data is available from 31 March 2015 and is provided with a latency of about 12 h.

SMOS and SMAP observe in a restricted band (1.400-1.427 GHz) reserved for passive radioastronomical use. Nevertheless, there are surfaced based artificial sources causing RFI (Mecklenburg et al., 2012). The image reconstruction process required to obtain the SMOS TBs includes an inverse Fourier transform (Corbella et al., 2004). Therefore, not only the grid cells that contain the RFI source are affected, but the whole snapshot can be contaminated, resulting in high or even negative brightness temperatures (Oliva et al., 2012). Since in nature brightness temperature will not exceed 300 K over the polar ocean (Kaleschke et al., 2010; Mills and Heygster, 2011; Tian-Kunze et al., 2014), a simple RFI filter is to eliminate the whole snapshot which contains at least one TB exceeding this threshold. This filter is used in sea ice thickness retrieval algorithm presented in

Huntemann et al. (2014). An alternative approach for filtering RFI has been shown in Huntemann and Heygster (2015) where incidence angle binning is used, resulting in a higher preservation of data and fewer gaps on the grid. Since SMAP contains onboard hardware for detection and filtering of RFI and neighboring pixels are unaffected by a RFI source, no additional filtering is required for the SMAP Level 1B data.

3 Sea ice thickness retrieval using a fit function

Due to the new SMOS data version 6.20 used here compared to version 5.05 used in Huntemann et al. (2014), a retraining of the SMOS thin ice thickness retrieval is necessary. First, in Sect. 3.1 we use the method presented in Huntemann et al. (2014) just using the newer data version 6.20. This involves averaging the brightness temperatures between 40 and 50° incidence angle. Secondly, we employ a fitting function using the dependence of brightness temperature on incidence angle (Section 3.2) as input for the retrieval (Section 3.3). The fitting function is used to obtain SMOS brightness temperatures at a fixed incidence angle.

3.1 SMOS retrieval retraining

Three SMOS grid cells in the Kara and Barents Sea were used for training over a period of three months (1 October - 26 December 2010) with sea ice thickness data obtained using the relation with the Cumulated Freezing Degree Days (CFDD) based on NCEP temperature data (Huntemann et al., 2014). CFDD is the daily average temperature below -1.8° (freezing point of sea water), integrated over the time with sub freezing temperatures (Bilello, 1961). The relation beween the CFDD and the thickness as presented in Bilello (1961) is $SIT[cm] = 1.33 \cdot (\mathrm{CFDD}[^\circ C])^{0.58}$. The ASI (Spreen et al., 2008) Sea Ice Concentration (SIC) was used to filter low SIC data during the training period. Only during the early part of the freeze-up when ice is really thin, the SIC was allowed to have a value between 0-100% (Huntemann et al., 2014) otherwise 100% SIC was required. The brightness temperatures are averaged daily over the incidence angle range between 40° to 50°. The functions

$$\begin{aligned} I_{abc}(x) &= a - (a-b) \cdot \exp(-x/c), \\ Q_{abcd}(x) &= (a-b) \cdot \exp(-(x/c)^d) + b, \end{aligned} \tag{2}$$

are fitted to the I and Q data measured over the training areas and the SIT resulting from the CFDD method, where a, b, c and d represent the curves parameters (Table 1), x is the sea ice thickness while I and Q are the brightness temperature intensity and polarization difference, respectively. The sea ice thickness retrieval curve is the result of using the two fitted functions from Equation 2 in the (Q, I) space. For each pair of Q and I the minimum Euclidean distance to the retrieval curve is used to determine the SIT. The retrieval curve parameters for data version 5.05 presented in Table 1 are updated values of the Huntemann et al. (2014) that are currently used for daily processing at the University of Bremen (www.seaice.uni-bremen.de).

Figure 1 shows the retrieval curves in the (Q, I) space. The dots on the curves represent the SIT increasing with intensity and decreasing with polarization difference in steps of 10 cm from 0 cm to 50 cm. Over 50 cm the retrieval is too sensitive to small changes in intensity and polarization difference and it will be cut off. The sea ice thickness retrieval curve for data

version 5.05 and the retrained curve using the 6.20 data version are shown in black and blue, respectively. The new curve has about 1.7 K higher value at zero SIT for intensity and polarization difference. The difference increases up to 3 K at 50 cm SIT.

Figure 2 shows the intensity (left) for 29 October 2010 using daily mean TBs for each grid cell. The data has been regridded to the NSIDC polar stereographic grid with a resolution of 12.5 km. This resolution is a oversampling of the true resolution of the SMOS data which is 43 km on average. The original validated retrieval (Huntemann et al., 2014) was trained with the old data version and is used as a reference here. The warm bias of the new data is seen in the difference plot (Fig. 2 right) both over ocean area and sea ice. In regions of high contrast like the ice edge or coastlines, both data versions tend to produce spillover effects (SMOS Calibration team and Expert Support Laboratory Level 1, 2015). The spillover produces an erroneous increase or decrease in brightness temperature of 1 to 1.5 K in the areas mentioned (not visible in the plot).

The algorithm trained with SMOS data version 5.05 has been compared with the one trained with version 6.20 for the period 1 October to 26 December 2010, considering sea ice thicknesses from 1 cm to 50 cm. The bias of the new retrieval is -0.22 cm while the RMSD is 1.35 cm. From a total of 5.1 million cumulated data points over the 87 days period and 50 cm sea ice thickness range, 97% have at most 3 cm difference. The bias and standard deviation are below ± 1 cm and 2 cm, respectively, for ice thicknesses below 25 cm. For 50 cm thickness the bias increases to $+4$ cm while the standard deviation reaches 11 cm.

A test is done to estimate the error introduced by the usage of the original retrieval (Huntemann et al., 2014) with the 6.20 data version. The two algorithms trained with the different data versions have taken as input the 6.20 data only. The data covers the freeze-up period from 1 October to 26 December 2010. The bias between the retrained retrieval and the original one is 0.33 cm with 99% of the data having a difference of 3 cm or less, while the RMSD is 0.91 cm. This means, although it is recommended to use the algorithm adapted for the new data version, the error is below 1 cm thickness on average for SIT below 51 cm if processed with the old algorithm.

3.2 SMOS TBs fit characteristics

In the previous section, we have shown that the SIT retrievals with the new data version and new retrieval is consistent with the old data version and retrieval. In all of the next sections the SMOS Level 1C 6.20 data version will be used, and when making reference to the original daily mean sea ice thickness retrieval, the retrained 6.20 data version algorithm from Sect. 3.1 will be utilized. In each grid cell, the number of data points and the covered incidence angle range are highly variable due to the orbit characteristics, the large incidence angle range of 0° to 65°, and the complex distribution of incidence angle within a SMOS snapshot. Grid cells located closer to the center of the swath will cover a large incidence angle range. Near the swath edges, the range is reduced and low incidence angles are not covered (Font et al., 2010). The snapshots removed using the over 300 K RFI filter can create a local bias in the average incidence angle. The existence of an RFI source before an observed grid cell, relative to the trackline, will result in the elimination of snapshots with high incidence angle data points for that cell. As opposite, a RFI source located after the grid cell of interest will result in elimination of the low incidence angle data points. The varying angle distribution depending on the position in the swath and the data removal due to the RFI filtering for one grid cell may shift the average incidence angle of the ensemble of observations between 40° and 50° away from the assumed average of 45°. The average brightness temperatures and SIT values retrieved from the affected grid cells will be shifted accordingly.

This error can be avoided by fitting a curve to the angular dependent brightness temperatures, allowing to estimate brightness temperature for a fixed incidence angle to be used for the retrieval.

Here we propose as a solution a modified version of the fit functions (Eq. 3) described in Zhao et al. (2015). The fit is applied separately to each polarization, horizontal and vertical, for each grid cell using daily observations. An initial filtering of RFI is done by removing observations which are flagged in Level 1C data for either being affected by tails of point source RFI or for indicating RFI by the system temperature standard deviation exceeding the expected trend (Indra Sistemas S.A., 2014). The flagged data is removed before the brightness temperatures are transformed from the antenna to the earth reference frame.

The fit is done iteratively with a maximum of five steps. For each step the parameter C (Eq. 3) is determined for a given grid cell by first summing up the brightness temperatures of horizontal and vertical polarization for each individual observation and then taking the median of the result. Median is used so that any RFI influenced outliers will not influence C. Due to asymmetric change in TB between horizontal and vertical polarization at higher incidence angles, only grid cells with at least one observation under 40° are considered. This increases the stability of the fit since $C/2$ represents the intensity at nadir. The 40° threshold is selected due to increased asymmetry between vertical and horizontal brightness temperatures at higher incidence angles which will generate a bias in the computation of the parameter C. The other five fit parameters a_h, b_h, a_v, b_v and d_v in the fit functions

$$\begin{aligned} TB_h(\theta) &= a_h \cdot \theta^2 + \frac{C}{2} \cdot [b_h \cdot \sin^2(\theta) + \cos^2(\theta)] \\ TB_v(\theta) &= a_v \cdot \theta^2 + \frac{C}{2} \cdot [b_v \cdot \sin^2(d_v \cdot \theta) + \cos^2(d_v \cdot \theta)]. \end{aligned} \tag{3}$$

are determined by a least squares procedure. The Brewster angle effect on the vertically polarized TBs is represented by the additional parameter d_v.

At each iteration of the fitting procedure 20% of the observations with the highest absolute difference from the fit are removed if the RMSD of the fit is higher than 5 K or if the RMSD fit difference between successive iterations exceeds 1 K. The data removal in the iterative process is the second step used to discard possible RFI influences.

The fit function is not optimized for extrapolation of the covered incidence angle range. Incidence angles not covered by the observations will have high uncertainty. To avoid extrapolation, only grid cells which contain observations with incidence angle both below and above the desired angle, e.g. 45°, are used for the retrieval.

3.3 Sea ice thickness retrieval training using fitted data

The retrieval algorithm has been retrained as described in Sect. 3.1 but instead of using TBs averaged over 40-50° incidence angle, now we use brightness temperatures from the fit process (Sect. 3.2) at a nominal incidence angle of 45°. The resulting retrieval curve (Fig. 2 green) has 1.3 K higher polarization difference at 0 cm ice thickness than the algorithm trained with the daily mean data (blue). The difference decreases to 0.1 K at 20 cm thickness and increases to approximately 0.5 K at 50 cm. This can come from variability in mean incidence angle. The daily averaged observations have an incidence angle bias of -0.5° (with single differences as high as -2.5°) relative to the assumed 45° one. The smaller incidence angle will result in a smaller polarization difference since this decreases when approaching nadir. The ocean and thin sea ice have low intensities and high

polarization difference. As the sea ice gets thicker, the intensity increases and the polarization difference decreases. For the same incidence angle bias at higher thicknesses the polarization difference error will be smaller. The intensity values for the two curves at the same sea ice thickness are nearly the same. The difference between these two curves is small compared to the difference to the retrieval curve for the SMOS 5.05 data version (Fig. 2 black).

Figure 3 shows the retrieved sea ice thickness using the daily mean method (left) presented in Sect. 3.1 and the retrained retrieval curve at nominal 45° incidence angle (center) based on the fitted brightness temperatures for 29 October 2010. Due to the requirement for the fit computation to have observation below 40° (Sect. 3.2), some grid cells in the central Arctic are not covered anymore. The decrease is around 1° in latitude, corresponding to approximately 1000 grid cells. This area is mostly covered by ice with thickness higher than 50 cm thus not being the focus of the retrieval. On the other hand for many ocean areas which formerly were excluded by the RFI filtering (grey in Fig. 3 left) now data is available, e.g. around Iceland, Eastern Greenland and Vladivostok. At the same time in the area of the Hudson Bay there is a 30% decrease in the area covered due to not fulfilling the incidence angle criteria required for SIT retrieval or the failure of the least square procedure to converge to a solution. For 90% of the grid points the difference is less than 3 cm which is below the estimated retrieval error of 30% of SIT computed in Huntemann et al. (2014). The daily mean retrieval has a positive bias of 0.41 cm. The highest differences appear north of Alaska with values up to 10 cm (Fig. 4 right). This is a result of a biased distribution of the incidence angles, resulting in a large number of grid points having under 45° mean incidence angle. This decreases the polarization difference dragging the resulting SIT to higher values. Overall the RMSD for this day is 1.9 cm which is within the expected 30% error margin of the retrieval.

Figure 4 (top) represents the bias (blue) and RMSD (red) of the SIT based on the 45° incidence angle fitted TBs relative to the 40-50° daily mean SIT calculated for the period 1 October to 26 December 2010. This is computed by dividing the SIT into bins of 1 cm thickness, from 0 to 50 cm, selecting all grid cells with that thickness from the daily averaged SIT and subtracting them from the fitted TBs SIT. Only grid cells that contain at most 50 cm and non-zero in at least one of the two algorithms are used. Overall the SIT from the fitted TB is smaller than the SIT from the 40-50° incidence angle mean TB. Until 40 cm of thickness the bias varies between 0 and -1 cm and then increases gradually up to -5 cm at 50 cm SIT. The green curve shows the cumulative histogram for daily mean TB at each sea ice thickness. Approximately 52% of the data is below or equal to 3 cm in the daily averaged TB SIT. This can be explained by the coarse resolution of about 43 km of SMOS, always generating thin sea ice at the ice edge due to brightness temperature contamination from either the ocean or the ice pack. In addition also coastal areas will generate thin sea ice due to spillover effects. Overall we can see that 95% of all data is below 40 cm while thickness corresponding to just 40 and 50 cm are contained in 5% of the data so that the region of high bias is small. Figure 4 bottom shows the daily bias (blue) and RMSD (red) of the 45° fitted brightness temperatures SIT relative to the daily average TB SIT. Over the whole period the bias stays between 0 and -0.6 cm while the RMSD increases from 1.3 K to 2.5 K. The increase in RMSD can be explained by the freeze-up period which contains larger areas with intermediate thicknesses compared to the start and peak freeze-up periods which contain either ocean or over 50 cm SIT grid cells. The overall bias of the 45° fitted brightness temperatures SIT for the whole period for all thicknesses is -0.3 cm with a RMSD of 2.02 cm. The absolute bias for over 3 cm thicknesses is 1.6 cm.

4 Sea ice thickness retrieval using SMAP data

This section adapts the SMOS SIT algorithm to observations of SMAP. Because SMOS observations have a variable incidence angle, they have to be computed at the fixed incidence angle of SMAP using the fitting function method described in Section 3.2. In order to apply the SIT retrieval calibrated with SMOS data also to those of SMAP, first the brightness temperatures of both sensors have to be inter-calibrated (Sec. 4.1). In Section 4.2 the resulting inter-calibrated brightness temperatures are mixed and used for generating a combined SMOS/SMAP sea ice thickness dataset.

4.1 SMAP/SMOS inter-calibration

The first step is to retrain the SMOS retrieval as in Sect. 3.3 using the nominal incidence angle of 40°, which is the fixed incidence angle of SMAP. The resulting SIT retrieval curve is shown in red in Fig. 1. As expected, the lower incidence angle results in a lower polarization difference especially for thin ice and reduces the usable polarization difference range for the retrieval from 22-54 K to 17-43 K.

A procedure to convert between SMOS and SMAP TBs over land was previously suggested in Lannoy et al. (2015). It uses a radiative transfer model and auxiliary data for taking in account atmospheric and galactic contributions for SMOS. For interpolation of SMOS TBs to 40° incidence angle it fits a quadratic function to the angular dependent SMOS TBs.

In this study the procedure to convert from SMAP brightness temperatures to SMOS equivalent TBs is done through simple linear regression. For the procedure we use SMOS 40° measurements data and SMAP L1B TOA observations for the period between 1 October to 31 December 2015, which covers the first freeze-up in the Arctic observed by both sensors. In the first step, the SMAP data is gridded daily on the SMOS ISEA 4H9 grid (the native SMOS Level 1C data grid) using a Gaussian resampling with a cutoff distance from the grid cell center of 20 km and Full Width Half Maximum (FWHM) range of 40 km. Only grid cells located more than 100 km away from the coast are considered to minimize the land contamination. In the second step we determine the fit function parameters for the SMOS data on a daily basis and compute the 40° SMOS TBs for each grid cell for each day. Figure 5 shows the scatter plots between the TBs of SMAP and SMOS 40° for horizontal (left) and vertical (right) polarization. For each polarization the magenta line shows the linear regression. We can distinguish two areas of high data point density at the two ends of the clouds open water and for thick sea ice, respectively. Over open water at a brightness temperature of 80 K and 120 K for TB_h and TB_v, respectively, SMOS has a warm bias of approximately 3.3 K and 5.2 K. At the high brightness temperatures representing the solid ice cover, the bias for SMOS decreases to 2.7 K and 3.3 K for TB_h and TB_v, respectively. The bias of SMOS TBs in the 6.20 data version that is presented in Section 2 can be one of the sources for the difference between SMOS and SMAP TBs. The asymmetry between low TBs and high TBs can come from the high and low reflectivities of ocean and sea ice, respectively at L-band. Unlike SMAP, SMOS data does not include correction for galactic noise which can have a higher influence over water due to its high reflectivity. The reflectivity decreases over sea ice, resulting in galactic noise having a smaller impact on recorded values thus lower differences between corrected and uncorrected TBs. The overall RMSD of the two linear regressions is 2.7 K and 2.81 K for TB_h and TB_v, respectively. The resulting linear regression parameters are presented in Table 2.

For this study, in order to use SMAP data for SIT retrieval, we adjust the SMAP TBs by a linear regression to 40° SMOS incidence angle data. A similar calibration of SMAP to SMOS TBs was presented previously in Huntemann et al. (2016). For that calibration, however, the SMAP Level 1C TB product was used which contains surface brightness temperatures on a 36 km EASE grid. They contain an atmospheric correction unlike the TOA Level 1B data that is used in the current paper. Also, the calibration is done through two separate linear regressions. The SMAP and SMOS 38-42° incidence angle data is daily averaged and compared for the period 1 October to 31 December 2015 (Sect. 4.1). In the second step, since the SMOS SIT retrieval algorithm used in Huntemann et al. (2016) was developed for 40-50° daily averaged data another calibration is required. Using SMOS L1C data for the same period, a linear regression is done between SMOS 40-50° and SMOS 38-42° daily averaged data. The main differences between the Huntemann et al. (2016) and the current paper is that here the SIT retrieval has been retrained to the fixed incidence angle of 40° and is not necessary anymore to correlate SMAP TBs with the 40-50° SMOS averaged TBs. Instead we retrain the retrieval to work directly with 40° TBs. Since the incidence angle difference between the SMAP data and the SMOS 40-50° does not need to be corrected anymore, the calibration that is done in the current paper is necessary to compensate for extraterrestrial contributions that are corrected in SMAP data and for the warm bias of the SMOS data. The RMSD for the linear relation between SMAP and SMOS data in Huntemann et al. (2016) is over 4 K for both polarizations, with at least 1.3 K higher than the one presented in this paper.

For a daily sea ice thickness retrieval, based on SMAP brightness temperatures only, both horizontal and vertical, are first adjusted to the SMOS brightness temperature using the linear regression parameters. Then they are gridded into a 12.5 km resolution NSIDC polar stereographic grid using a Gaussian weighting for the distance with a cutoff from the grid cell center of 15 km and FWHM range of 40 km. For the period from 1 October to 31 December 2015, the difference in sea ice thickness between SMOS 40° incidence angle fitted TBs retrieval and SMAP retrieval are small, 2.39 cm RMSD and -0.2 cm average difference for the SMOS SIT relative to the SMAP retrieval taking into account only grid cells containing at most 50 cm SIT and at least one of the two retrievals having over 0 cm.

4.2 SMOS/SMAP combined sea ice thickness retrieval

Because of the small differences of the retrievals from the two sensors, combined maps are produced using both of them. The daily mean horizontal and vertical brightness temperatures are computed separately for both sensors. For each grid point of the SMOS ISEA 4H9 grid we compute the daily SMOS TBs using the 40° fit. Then the brightness temperatures are regridded to the NSIDC 12.5 km grid commonly used for sea ice maps. SMAP brightness temperature data is gridded directly to the NSIDC grid using a Gaussian resampling as was done in Sect. 4.1. The two resulting TB datasets are averaged. Finally the sea ice thickness retrieval for 40° incidence angle is applied. The result is a SIT map that has the benefit of using data from both sensors (e.g. Fig. 6 (left)) it has a larger coverage, and is less affected by RFI sources. For the area north of 55.7°N the coverage in the mixed dataset increases over 6% compared to the 40-50° daily mean TB retrieval. Also the combined brightness temperatures are more representative for a daily mean due to the 12 hours difference in the equator crossing time between the two sensors. The RMSD between the original 40° to 50° incidence angle daily mean retrieval from Sect. 3.1 and the new mixed sensor one is 2.05 cm for the 1 October to 31 December 2015 period investigated, while the bias is -0.58 cm. The result means

that the mixed sensor SIT is on averaged slightly smaller than the SMOS daily averaged brightness temeratures SIT. Figure 6 center shows the difference between SMOS 40-50° incidence angle averaged TBs sea ice thickness and the mixed data for 24 October 2015. The highest differences appear mostly in the transition area of 40 cm to over 50. Taking in account just data points with maximum value of 50 cm and for at least one of the two datasets a value over 0 cm, the 93% of the data has an absolute difference of at most 2 cm for the three months period compared. Figure 6 right compares the retrieval done just with the SMOS 40° fitted brightness temperatures to the mixed data one. For this comparison, the averaged difference is below -0.1 cm and the RMSD is 1.37 cm for the complete three months period.

5 Assessment of uncertainties

5.1 Sea ice thickness uncertainties

In the SIT retrieval using 40° incidence angle TBs of the two sensors several factors contribute to the uncertainty: the radiometric accuracy of the observations, RFI contamination in the TB data, the uncertainty in the auxiliary data used for the training of the retrieval, the influence of the SIC on the TBs and the sub-daily variability of the TBs themselves.

Here we propose a method to quantify the uncertainty of the retrieval. We first compute the SIT in the (TB_h, TB_v) space using the 40° TBs trained retrieval (Fig. 7 (left)). The TBs that will be used in a retrieval will more likely be found above the one-to-one line (black line) where the vertical brightness temperature is higher than the horizontal one. The color in the diagram indicates the retrieved SIT according to the retrieval curve for 40° incidence angle (red curve in Fig. 1). The TB space covered by the 40 to 50 cm thickness is small compared with the rest of the thickness range.

As second step we compute the derivative of SIT as a function of TB_h and TB_v seen in Fig. 7 center and right, respectively. Almost all of the data points will be found above the one-to-one line where the polarization difference is positive. For most of TB_hs below 200 K the rate of change of the SIT is below 0.5 cm per K and is increasing sharply with increased TB_h at over 230 K TB_v. In contrast, the derivative for TB_v (Fig. 7 right) at values above 230 K is positive for TB_h below 213 K, and becomes negative above it. The sensitivity of SIT relative to TB_h and TB_v will be used to compute the uncertainty of the retrieval. For a given pair (TB_h, TB_v) and their associated uncertainties we compute the SIT and corresponding SIT uncertainties:

$$sigma_{SIT} = \sqrt{\left(\frac{\partial SIT}{\partial TB_h}\right)^2 \cdot \sigma^2_{TB_h} + \left(\frac{\partial SIT}{\partial TB_v}\right)^2 \cdot \sigma^2_{TB_v} + 2 \cdot \left(\frac{\partial SIT}{\partial TB_h}\right) \cdot \left(\frac{\partial SIT}{\partial TB_v}\right) \cdot \sigma_{TB_h} \cdot \sigma_{TB_v} \cdot \rho_{TB_h TB_v}} \quad (4)$$

where σ_{TB_v} and σ_{TB_v} represent the TB uncertainties, $\rho_{TB_h TB_v}$ is the correlation between the two polarizations. The values of the SIT derivatives are taken from the second step of the method for each pair of (TB_h, TB_v).

For this study we do not take into account the radiometric accuracy of either sensor because they are small compared to the other errors, especially the brightness temperature variation during one day. For each SMOS observation at 40°incidence angle, the TB uncertainty is assumed to be the RMSD resulting from the fitting process presented in Sect. 3.2. During the fitting routine the RMSD is computed for each iteration and a 5 K threshold is used for eliminating outliers. Although this process is used to eliminate potential RFI influences in the data, it will also reduce the variability that comes from observations of the

same grid cell at different times of the day. For SMAP brightness temperatures a weighted standard deviation for each grid cell using all observations from one day is used as uncertainty. The correlation between the TB_h and TB_v is 0.81 and 0.97 for SMOS and SMAP, respectively. The correlation was calculated for a period of seven days. It was computed per day over the whole Arctic using daily averaged TB for each grid cell and is consistent during the whole period.

Figure 8 shows as an example the scatter plot and moving average (red lines) of the SIT uncertainty (Eq. 4) for 11 October 2015 for SMOS (top) and SMAP (bottom). The restrictions imposed on the RMSD of the SMOS data have a clear impact on results. The TB uncertainties for SMOS in majority over 2 K lead at higher thicknesses to high uncertainty. Because the SMAP data is still containing the full variability of observations of one day, there will be grid cells with over 5 K uncertainty, but overall the median is around 1.2 K, in comparison with SMOS where the uncertainties are clustered around 4 K. Again, the smaller uncertainty of the SMOS data is only due to the TB fitting procedure, which removes outliers. Without that, for the raw data, the SMOS uncertainty would be similar or even larger than for SMAP. For both sensors we can observe a rapid increase of the uncertainties beyond 35 cm SIT (Fig. 8).

5.2 Sea Ice Concentration impact

The SIT retrieval used in this paper assumes 100% ice concentration. As a result, the retrieved sea ice thickness decrease if this condition is not fulfilled. We assume that brightness temperature over sea ice varies linearly with the change in sea ice concentration:

$$TBp(SIT, IC) = TBp_i(SIT) \cdot IC + TBp_w \cdot (1 - IC) \tag{5}$$

where p represents the polarization, TBp_i and TBp_w are the brightness temperatures of ice and water, respectively and IC is the sea ice concentration.

For this study we first use 40° SMOS brightness temperatures from 11 October 2015 for retrieval. The resulting SIT will be considered the assumed sea ice thickness. In the second step we take the same TBs as input for TBp_i, use fixed tie points for TBp_w with 85 K and 125 K as values for the horizontal and vertical TBs, respectively. For each pair of SMOS and water brightness temperatures we consider a range of sea ice concentrations for which we compute SIT using Eq. 5. The assumed SIT is grouped in bins of 1 cm thickness. Its corresponding thicknesses from the second step are averaged for each SIC separately. Figure 9 shows how the retrieved SIT varies relative to the assumed SIT depending on the SIC. For a SIC of 90% at 10 cm the retrieved SIT is 8.5 cm, while at 50 cm is just 28 cm.

Current retrievals for SIC are influenced by thin sea ice. In Heygster et al. (2014), SIC algorithms have been tested for 100% sea ice concentration with thicknesses below 50 cm. All algorithms show less than 100% SIC for thicknesses below 30 cm. In another study done by Ivanova et al. (2015) all SIC algorithms registered a decrease in SIC, up to 60% at 5 cm, and an overall bias of 5% for over 30 cm. As we have observations at two polarizations at each grid cell available, it should in principle be possible to retrieve SIT and ice concentration simultaneously. However, an attempt has shown a strong noise increase in SIT (Kaleschke et al., 2013).

During the winter most of the Arctic is covered by SIC of 90% and higher (Andersen et al., 2007). For an assumed uncertainty of the sea ice concentration data of 4% (Ivanova et al., 2015) the error that could be introduced by a correction of sea ice thickness for high SIC is higher than that of the error introduced by the assumption of 100% sea ice concentration (Tian-Kunze et al., 2014). The uncertainty of SIC algorithms at high concentration and their covariation at thin thicknesses will cause high errors if a correction to SIT is applied using current SIC datasets. As a result full ice cover is assumed for the SIT retrieval.

6 Conclusions

The existing retrieval for thickness of thin sea ice (Huntemann et al., 2014) from the L-band sensor SMOS (launched 2009) has been adapted to SMAP (launched 2015) by (i) modifying the SMOS retrieval to use 40° incidence angle instead of the average in the range 40° to 50°, (ii) establishing a linear regression between the SMOS and SMAP brightness temperatures at 40° incidence angle.

To derive the SMOS brightness temperature at 40° incidence angle required for the first step, an analytical function is fitted to the incidence angle dependent brightness temperatures. SMAP top of the atmosphere data and the SMOS data fitted to the same incidence angle yield a small TB RMSD between the two datasets for both polarizations of 2.7 K and 2.81 K for TB_h and TB_v, respectively. This is an improvement compared to previous attempts (Huntemann et al., 2016) where the RMSD for both polarizations was over 4 K. Moreover the SMOS based ice thickness retrieval has been adjusted to the new SMOS data version 6.20. The new algorithm contains a new RFI filtering routine exploiting the dependence of the brightness temperatures on the incidence angle. This method improved coverage of previously RFI affected areas. Although the TB datasets of the two sensors are processed differently, the overall resulting thicknesses are similar, with SMOS TBs having smaller variability at lower thicknesses due to the iterative observations removal operation, .

Concluding, the benefit of SMAP for retrieval of thickness of thin sea ice is twofold: first, the combined product has a better spatial and temporal coverage that in future studies can allow insights even on a sub-daily scale. The overall increase in spatial coverage is 6%. Second, SIT can be retrieved from any of the two sensors alone with similar accuracy, making the production chain more stable in the case of malfunction of one of the two sensors. The small differences in retrieved SIT between the presented method and the method from Huntemann et al. (2014) allows us to refer to their comparisons for the assessment of the quality of this product. A full validation of the current retrieval requires a comparison with independent in-situ sea ice thickness data currently not available at the scales of thickness (below 50 cm) and horizontal extent of the sensor footprint (~43 km diameter).

Data availability. https://seaice.uni-bremen.de

Competing interests. No competing interests are present

Acknowledgements. We gratefully acknowledge the support from the Transregional Collaborative Research Center (TR 172). "ArctiC Amplification: Climate Relevant Atmospheric and SurfaCe Processes, and Feedback mechanisms $(AC)^3$" funded by the German Research Foundation (DFG, Deutsche Forschungsgemeinschaft).

References

Andersen, S., Tonboe, R., Kaleschke, L., Heygster, G., and Pedersen, L. T.: Intercomparison of passive microwave sea ice concentration retrievals over the high-concentration Arctic sea ice, Journal of Geophysical Research: Oceans, 112, 2007.

Bilello, M. A.: Formation, growth, and decay of sea-ice in the Canadian Arctic Archipelago, Arctic, 14, 2–24, 1961.

Castro, R.: Analytical Pixel Footprint, Technical note, available at: http://smos.com.pt/downloads/release/documents/SO-TN-DME-L1PP-0172-Analytical-Pixel-Footprint.pdf (last access: 6 April 2017), 2008.

Corbella, I., Duffo, N., Vall-llossera, M., Camps, A., and Torres, F.: The visibility function in interferometric aperture synthesis radiometry, IEEE Transactions on Geoscience and Remote Sensing, 42, 1677–1682, 2004.

Entekhabi, D., Njoku, E. G., O'Neill, P. E., Kellogg, K. H., Crow, W. T., Edelstein, W. N., Entin, J. K., Goodman, S. D., Jackson, T. J., Johnson, J., Kimball, J., Piepmeier, J. R., Koster, R. D., Martin, N., McDonald, K. C., Moghaddam, M., Moran, S., Reichle, R., Shi, J. C., Spencer, M. W., Thurman, S. W., Tsang, L., and Zyl, J. V.: The Soil Moisture Active Passive (SMAP) Mission, Proceedings of the IEEE, 98, 704–716, 2010.

Entekhabi, D., Yueh, S., O'Neill, P., Kellogg, K., Allen, A., Bindlish, R., Brown, M., Chan, S., Colliander, A., Crow, W. T., et al.: SMAP handbook, Tech. rep., available at: https://smap.jpl.nasa.gov/files/smap2/SMAP_Handbook_FINAL_1_JULY_2014_Web.pdf, 2014.

Font, J., Camps, A., Borges, A., Martin-Neira, M., Boutin, J., Reul, N., Kerr, Y. H., Hahne, A., and Mecklenburg, S.: SMOS: The Challenging Sea Surface Salinity Measurement From Space, Proceedings of the IEEE, 98, 649–665, 2010.

Heygster, G., Huntemann, M., Ivanova, N., Saldo, R., and Pedersen, L. T.: Response of passive microwave sea ice concentration algorithms to thin ice, in: 2014 IEEE Geoscience and Remote Sensing Symposium, pp. 3618–3621, 2014.

Holland, M. M., Serreze, M. C., and Stroeve, J.: The sea ice mass budget of the Arctic and its future change as simulated by coupled climate models, Climate Dynamics, 34, 185–200, 2010.

Huntemann, M. and Heygster, G.: A New Method to Filter Out Radio-Frequency Interference (RFI) from SMOS Level 1C Data for Sea Ice Applications, in: Towards an Interdisciplinary Approach in Earth System Science, edited by Lohmann, G., Meggers, H., Unnithan, V., Wolf-Gladrow, D., Notholt, J., and Bracher, A., pp. 91–98, Springer International Publishing Switzerland, 2015.

Huntemann, M., Heygster, G., Kaleschke, L., Krumpen, T., Makynen, M., and Drusch, M.: Empirical sea ice thickness retrieval during the freez-up period from SMOS high incident angle observations, The Cryosphere, 8, 439–451, 2014.

Huntemann, M., Patilea, C., and Heygster, G.: Thickness of thin sea ice retrieved from SMOS and SMAP, in: Proceedings of 2016 IEEE International Geoscience and Remote Sensing Symposium (IGARSS), pp. 5248–5251, 2016.

Häkkinen, S.: A constitutive law for sea ice and some applications, Mathematical Modelling, 9, 81–90, 1987.

Indra Sistemas S.A.: SMOS Level 1 and Auxiliary Data Products Specifications, Product Document, available at: https://earth.esa.int/documents/10174/1854583/SMOS_L1_Aux_Data_Product_Specification (last access: 28 March 2018), Madrid, 2014.

Ivanova, N., Pedersen, L. T., Tonboe, R. T., Kern, S., Heygster, G., Lavergne, T., Sørensen, A., Saldo, R., Dybkjær, G., Brucker, L., and Shokr, M.: Inter-comparison and evaluation of sea ice algorithms: towards further identification of challenges and optimal approach using passive microwave observations, The Cryosphere, 9, 1797–1817, 2015.

Kaleschke, L., Maaß, N., Haas, C., Hendricks, S., Heygster, G., and Tonboe, R. T.: A sea-ice thickness retrieval model for 1.4 GHz radiometry and application to airborne measurements over low salinity sea-ice, The Cryosphere, 4, 583–592, 2010.

Kaleschke, L., Tian-Kunze, X., Maaß, N., Mäkynen, M., and Drusch, M.: Sea ice thickness retrieval from SMOS brightness temperatures during the Arctic freeze-up period, Geophysical Research Letters, 39, l05501, 2012.

Kaleschke, L., Tian-Kunze, X., Maaß, N., Heygster, G., Huntemann, M., Wang, H., Hendricks, S., Krumpen, T., Tonboe, R., Mäkynen, M., and Haas, C.: STSE-SMOS Sea Ice Retrieval Study (SMOSIce), Technical Report, available at: https://icdc.cen.uni-hamburg.de/fileadmin/user_upload/icdc_Dokumente/SMOS_SIT/SMOSICE_FinalReport_2013.pdf (last access: 31 March 2018), ESA ESTEC, 2013.

Kerr, Y. H., Waldteufel, P., Wigneron, J. P., Martinuzzi, J., Font, J., and Berger, M.: Soil moisture retrieval from space: the Soil Moisture and Ocean Salinity (SMOS) mission, IEEE Transactions on Geoscience and Remote Sensing, 39, 1729–1735, 2001.

Kerr, Y. H., Waldteufel, P., Richaume, P., Wigneron, J. P., Ferrazzoli, P., Mahmoodi, A., Bitar, A. A., Cabot, F., Gruhier, C., Juglea, S. E., Leroux, D., Mialon, A., and Delwart, S.: The SMOS Soil Moisture Retrieval Algorithm, IEEE Transactions on Geoscience and Remote Sensing, 50, 1384–1403, 2012.

Lannoy, G. J. M. D., Reichle, R. H., Peng, J., Kerr, Y., Castro, R., Kim, E. J., and Liu, Q.: Converting Between SMOS and SMAP Level-1 Brightness Temperature Observations Over Nonfrozen Land, IEEE Geoscience and Remote Sensing Letters, 12, 1908–1912, 2015.

Maykut, G. A.: Energy exchange over young sea ice in the central Arctic, Journal of Geophysical Research: Oceans, 83, 3646–3658, 1978.

Mecklenburg, S., Drusch, M., Kerr, Y. H., Font, J., Martin-Neira, M., Delwart, S., Buenadicha, G., Reul, N., Daganzo-Eusebio, E., Oliva, R., and Crapolicchio, R.: ESA's Soil Moisture and Ocean Salinity Mission: Mission Performance and Operations, IEEE Transactions on Geoscience and Remote Sensing, 50, 1354–1366, 2012.

Mills, P. and Heygster, G.: Sea Ice Emissivity Modeling at L-Band and Application to 2007 Pol-Ice Campaign Field Data, IEEE Transactions on Geoscience and Remote Sensing, 49, 612–627, 2011.

Moritz, R. E., Bitz, C. M., and Steig, E. J.: Dynamics of Recent Climate Change in the Arctic, Science, 297, 1497–1502, 2002.

Oliva, R., Daganzo, E., Kerr, Y. H., Mecklenburg, S., Nieto, S., Richaume, P., and Gruhier, C.: SMOS Radio Frequency Interference Scenario: Status and Actions Taken to Improve the RFI Environment in the 1400-1427-MHz Passive Band, IEEE Transactions on Geoscience and Remote Sensing, 50, 1427–1439, 2012.

Perovich, D. K., Grenfell, T. C., Light, B., and Hobbs, P. V.: Seasonal evolution of the albedo of multiyear Arctic sea ice, Journal of Geophysical Research: Oceans, 107, SHE 20–1–SHE 20–13, 2012.

Sahr, K., White, D., and Kimerling, A. J.: Geodesic Discrete Global Grid Systems, Cartography and Geographic Information Science, 30, 121–134, 2003.

Skou, N. and Hoffman-Bang, D.: L-band radiometers measuring salinity from space: atmospheric propagation effects, IEEE Transactions on Geoscience and Remote Sensing, 43, 2210–2217, 2005.

SMOS Calibration team and Expert Support Laboratory Level 1: SMOS L1OPv620 release note, Release Note, available at: https://earth.esa.int/documents/10174/1854503/SMOS_L1OPv620_release_note (last access: 9 February 2018), ESA, 2015.

Spreen, G., Kaleschke, L., and Heygster, G.: Sea ice remote sensing using AMSR-E 89-GHz channels, Journal of Geophysical Research: Oceans, 113, 2008.

Stroeve, J., Holland, M. M., Meier, W., Scambos, T., and Serreze, M.: Arctic sea ice decline: Faster than forecast, Geophysical Research Letters, 34, 2007.

Tian-Kunze, X., Kaleschke, L., Maaß, N., Mäkynen, M., Serra, N., Drusch, M., and Krumpen, T.: SMOS-derived thin sea ice thickness: algorithm baseline, product specifications and initial verification, The Cryosphere, 8, 997–1018, 2014.

Yu, Y., Rothrock, D. A., and Zhang, J.: Thin ice impacts on surface salt flux and ice strength: Inferences from advanced very high resolution radiometer, Journal of Geophysical Research: Oceans, 106, 13 975–13 988, 2001.

Zhao, T. J., Shi, J. C., Bindlish, R., Jackson, T. J., Kerr, Y., Cosh, M. H., Cui, Q., Li, Y. Q., Xiong, C., and Che, T.: Refinement of SMOS multiangular brightness temperature toward soil moisture retrieval and its analysis over reference targets, IEEE Journal of Selected Topics in Applied Earth Observations and Remote Sensing, 8, 589–603, 2015.

Zine, S., Boutin, J., Font, J., Reul, N., Waldteufel, P., Gabarro, C., Tenerelli, J., Petitcolin, F., Talone, J. V. M., and Delwart, S.: Overview of the SMOS sea surface salinity prototype processor, IEEE-Transactions on Geoscience and Remote Sensing, 46, 621–645, 2008.

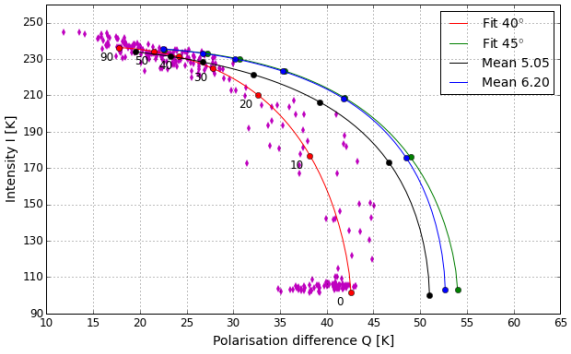

Figure 1. Sea Ice Thickness retrieval curves derived from SMOS data representing original algorithm (black), new data version (blue), 45° (green) and 40° (red) incidence angle fitted brightness temperatures. Dots represent data from the three training areas used for obtaining the 40° fit curve. Numbers under the curve represent the SIT in centimeters.

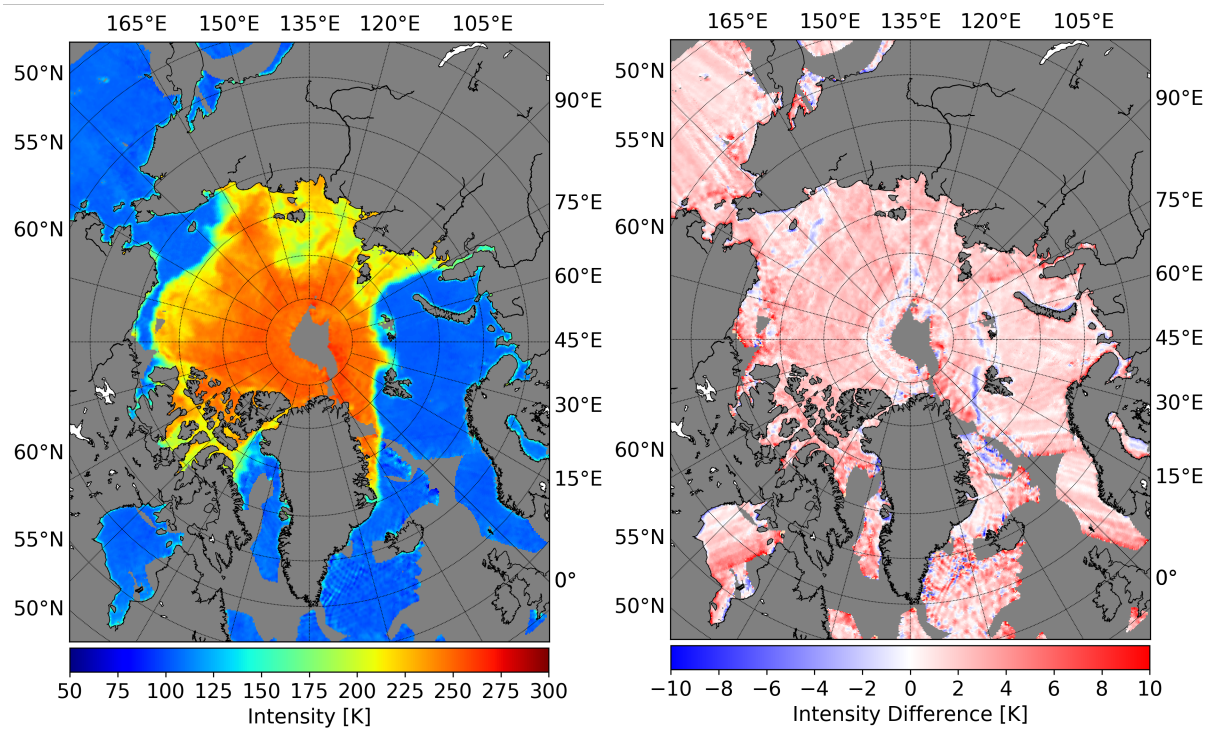

Figure 2. SMOS intensity for data version 6.20 data (left) for 29 October 2010 ; intensity difference (right) between the 6.20 and the 5.05 data versions.

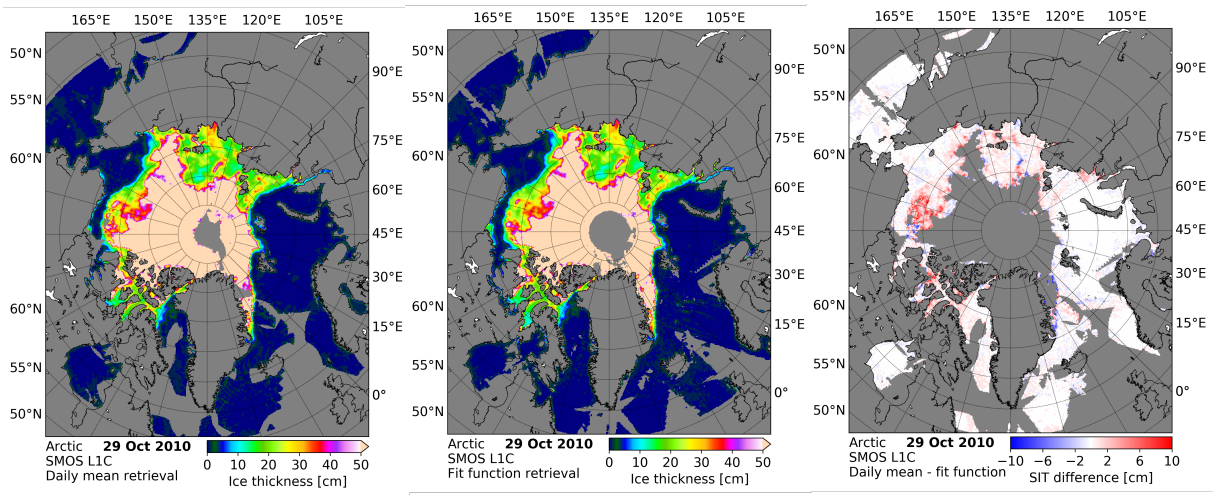

Figure 3. SMOS sea ice thickness retrieved on 29 October 2010 using 6.20 retrieval (left), retrieval using 45° incidence angle fitted brightness temperatures (central), and the difference between the two (right) with areas over 50 cm SIT not shown.

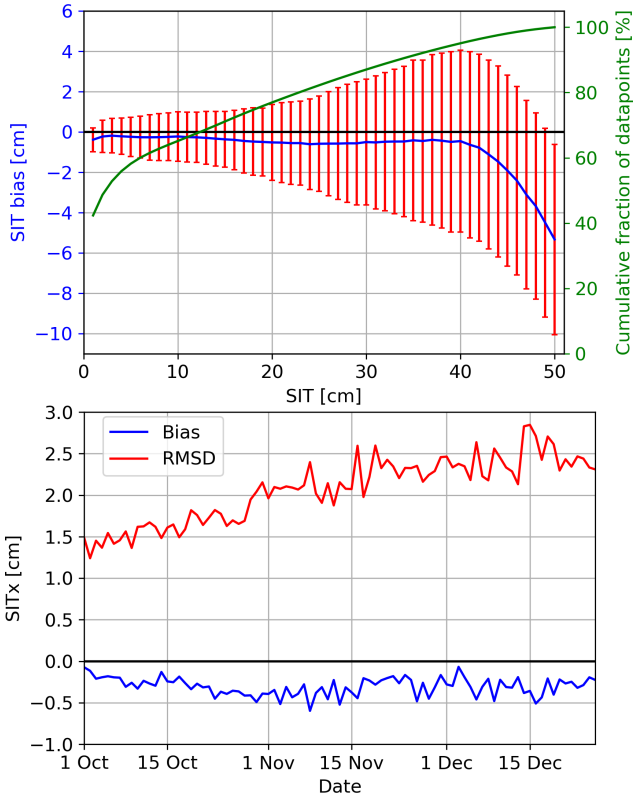

Figure 4. (Top) SIT bias (blue) calculated by substracting the SIT computed using 40-50° daily average from SIT using TBs fitted at 45° for the 1 Oct. to 26 Dec. 2010 period. Bias is computed relative to the daily average SIT in bins of 1 cm and its coresponding RMSD (red). Green curve represents the fraction from the total amount of data points for each thickness bin. Bottom figure shows the bias (blue) and RMSD (red) for each day separately.

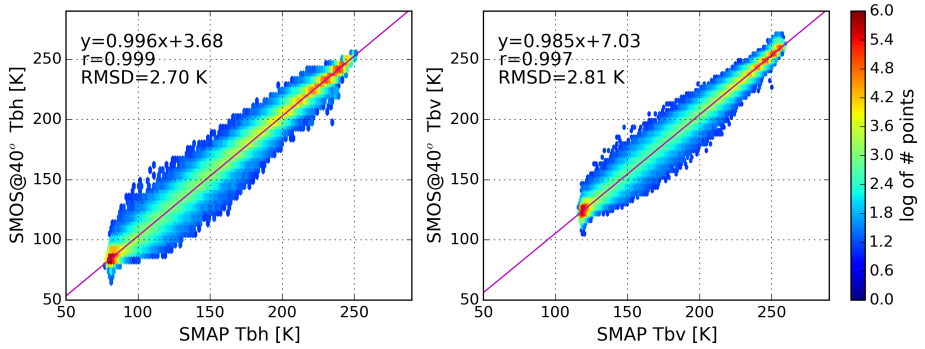

Figure 5. Logarithmic density plot of TB_h (left) and TB_v (right) data from SMAP and SMOS for the period 1 October to 31 December 2015. Magenta lines represent the linear regression between the two datasets.

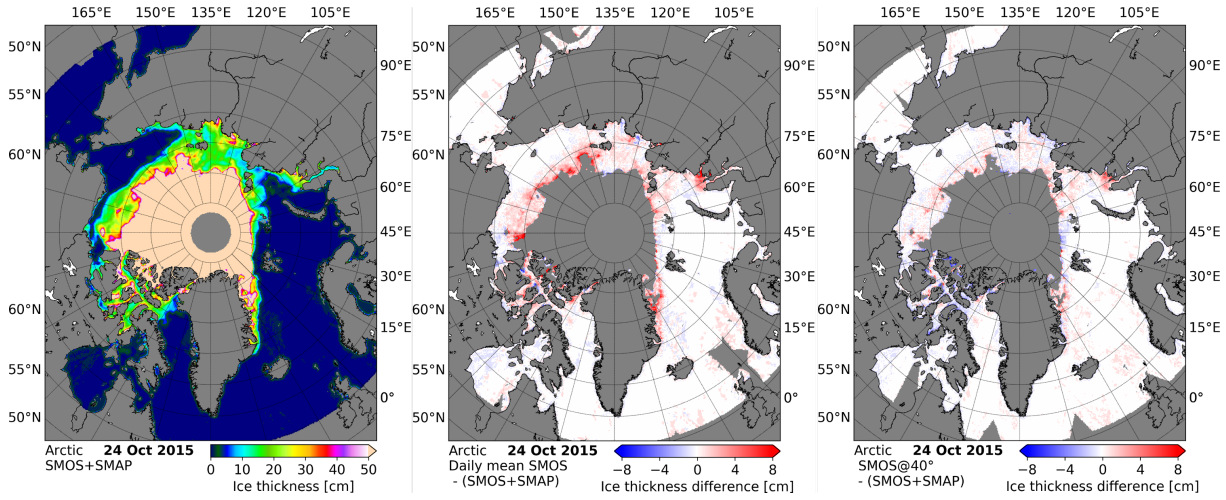

Figure 6. Sea Ice Thickness retrieved on 24 October 2015 for the joint SMOS+SMAP product (left), the SIT difference between the SMOS daily mean retrieval and the joint retrieval (center), and the SIT difference between SMOS fitted TBs at 40° incidence angle and the joint retrieval (right).

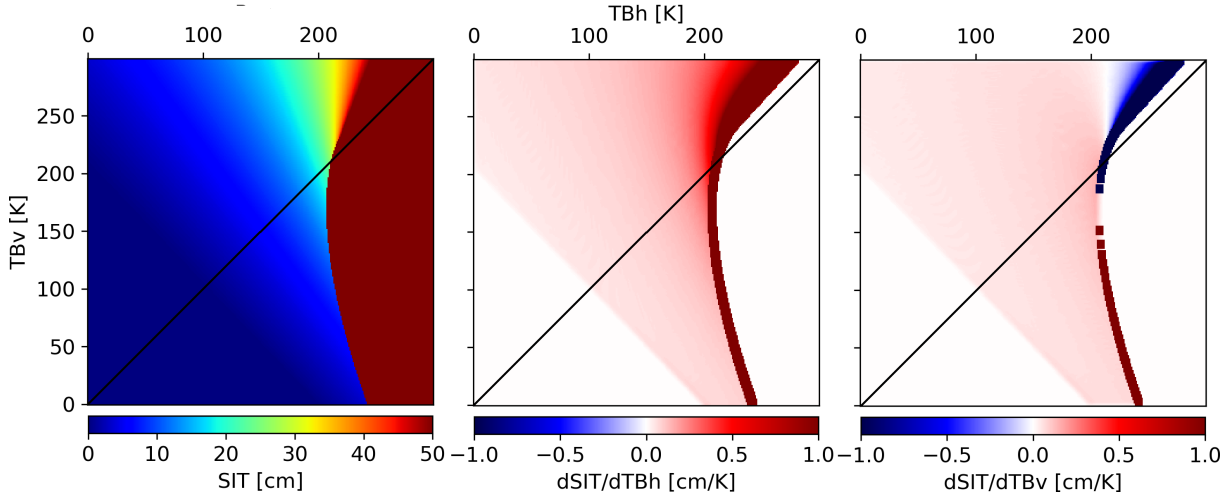

Figure 7. SIT (left) computed with the 40° TB algorithm (Fig. 1 red curve) represented in the space of TB_h and TB_v. Derivative of SIT as a function of TB_h (center) and TB_v (right). Black line represents the location of equal TB_h and TB_v, with the area above the line (TB_v higher than TB_h) representing values found in observations.

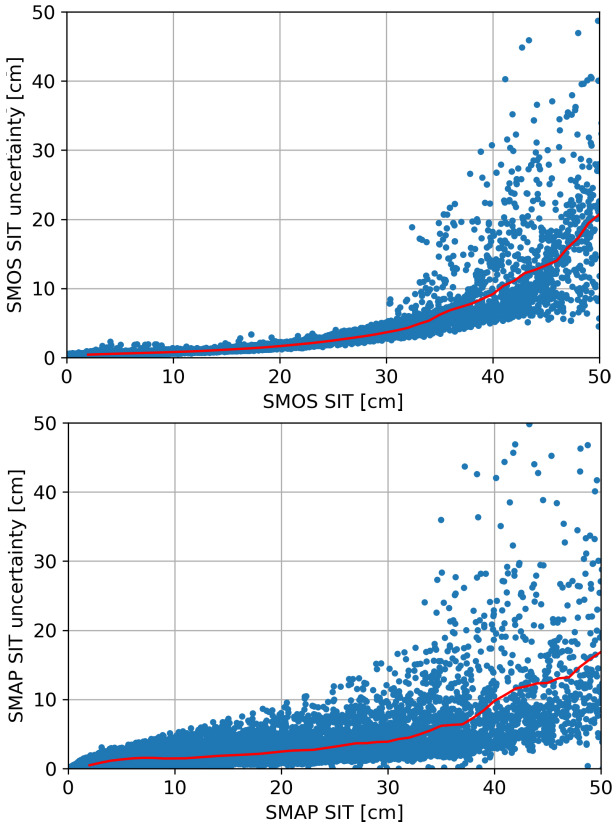

Figure 8. Scatter of SMOS (top) and SMAP (bottom) retrievals at 40°incidence angle for 11 Oct. 2015 in the Arctic and their respective uncertainties. Red line represent the rolling average of the uncertainty.

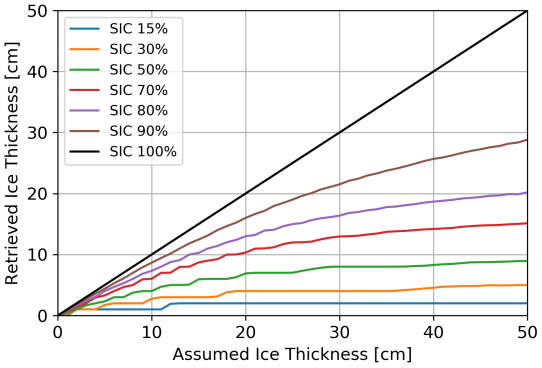

Figure 9. SIT retrieved as function of the assumed SIT under different SIC values.

Table 1. Sea ice thickness retrieval curve parameters for the original 5.05 data version training, 6.20 training, and the two fit curve parameters for 40° and 45° incidence angle

Retrieval	Parameter	a [K]	b [K]	c [cm]	d
5.05	I_{abc}	234.1	100.2	12.7	-
	Q_{abcd}	51.0	19.4	31.8	1.65
6.20	I_{abc}	235.7	103.0	12.7	-
	Q_{abcd}	52.7	22.3	33.2	1.60
fit 40°	I_{abc}	236.4	101.5	12.2	-
	Q_{abcd}	42.6	17.3	32.9	1.39
fit 45°	I_{abc}	235.4	103.3	12.5	-
	Q_{abcd}	54.0	22.2	33.0	1.47

Table 2. Parameters for linear regression between SMOS and SMAP brightness temperatures

Polarization	Slope	Intercept [K]	RMSD [K]	r
H	0.996	3.68	2.70	0.999
V	0.985	7.03	2.81	0.997